OPTO-ELECTRONICS REVIEW **14**(1), 61–70

High-performance IR detectors at SCD present and future

O. NESHER* and P.C. KLIPSTEIN

Semi Conductor Devices (SCD), P.O. Box 2250, Haifa 31021, Israel

For over 27 years, SCD has been manufacturing and developing a wide range of high performance infrared detectors, designed to operate in either the mid-wave (MWIR) or the long-wave (LWIR) atmospheric windows. These detectors have been integrated successfully into many different types of system including missile seekers, time delay integration scanning systems, hand-held cameras, missile warning systems and many others. SCD's technology for the MWIR wavelength range is based on its well established 2D arrays of InSb photodiodes. The arrays are flip-chip bonded to SCD's analogue or digital signal processors, all of which have been designed in-house. The 2D focal plane array (FPA) detectors have a format of 320×256 elements for a 30-µm pitch and 480×384 or 640×512 elements for a 20-µm pitch. Typical operating temperatures are around 77–85 K. Five years ago SCD began to develop a new generation of MWIR detectors based on the epitaxial growth of antimonide based compound semiconductors (ABCS). This ABCS technology allows band-gap engineering of the detection material which enables higher operating temperatures and multi-spectral detection. This year SCD presented its first prototype FPA from this program, an InAlSb based detector operating at a temperature of 100 K. By the end of this year SCD will introduce the first prototype MWIR detector with a 640×512 element format and a pitch of 15 µm. For the LWIR wavelength range SCD manufactures both linear $Hg_{1-x}Cd_xTe$ (MCT) detectors with a line of 250 elements and time delay and integration (TDI) detectors with formats of 288×4 and 480×6. Recently, SCD has demonstrated its first prototype uncooled detector which is based on VO_x technology and which has a format of 384×288 elements, a pitch of 25 µm, and a typical NETD of 50 mK at F/1. In this paper, we describe the present technologies and products of SCD and the future evolution of our detectors for the MWIR and LWIR detection.

Keywords: digital detector, 480×384 element detector, 640×512 element detector, focal plane array, MCT, IR detector, InSb, InAlSb, superlattice, TDI, DDC.

1. Introduction

Second generation infrared (IR) detectors at SCD are based on InSb for the mid-wavelength IR (MWIR) atmospheric window (3–5 µm), and on mercury cadmium telluride (MCT) for the long-wavelength IR (LWIR) window (8–12 µm) [1]. In the past 27 years, SCD has developed and manufactured ten types of infrared detector, both with support from the Israeli MOD and in cooperation with Israeli institutions and companies such as the Technion, Soreq NRC, RICOR and RAFAEL. SCD's current production line includes MCT devices with up to 4806 elements operating in time delay and integration (TDI) mode and two dimensional (2D) InSb focal plane arrays (FPAs) with up to 640×512 elements, all available in various configurations including fully integrated detector-dewar-cooler (DDC) packages. Many DDC configurations were developed, in most of the cases to custom design; they range from very small low power and weight DDCs such as "Piccolo" [2] up to a very long TDI DDC for airborne applications with push-broom imaging, with 2048×16 elements [3].

SCD's 2D InSb FPAs have been in production since 1997 with the 320×256 element format and since 2000 in the larger format of 640×512 elements. SCD also specializes in solutions optimized for various types of application from hand held cameras up to missile warning systems (MWS). The various solutions are based on the special design of Dewars which can endure a large range of environmental conditions and on the many operational modes of the signal processor which supports all the applications.

The general requirements of the third generation of IR detectors are:

- high resolution (larger format and smaller pitch),
- advanced integrated readouts (digital, low noise),
- higher operating temperatures (> 77 K),
- high spatial uniformity,
- high temporal stability,
- multi-spectral detection.

In order to be able to meet the third generation requirements, SCD has started two main programs about five years ago which are both based on the mature technology of planar InSb 2D arrays. The first one is focused on the signal processor which is bonded directly to the detection material,

*e-mail: onesher@scd.co.il

The paper presented there appears in *Infrared Photoelectronics*, edited by Antoni Rogalski, Eustace L. Dereniak, Fiodor F. Sizov, Proc. SPIE Vol. 5957, 59570S (2005).

in this program we developed a family of digital readout integrated circuits (ROIC) with a 20-μm pitch which is called Sebastian [4,5]. The first product of this program has a format of 640×512 and it was first introduced in 2003. Since then many detectors were produced and have been integrated successfully into systems. The second product consists of 480×384 elements and since 2004 it has been manufactured in SCD's production line [6].

The second program is focused on the detection material and more specifically antimonide based compound semiconductor (ABCS) materials which are the basic technology for future detectors at SCD [7–9]. This technology which uses epitaxial thin film growth in SCD's MBE machine enables band gap engineering of the detection material and the design and optimization of various structures for high operating temperature, a small pitch size and multi-colour detection. The first product of this program is based on an epitaxial InSb film grown on top of an InSb substrate, enabling an operating temperature above 90 K with the same performance as achieved with implanted planar InSb at 80 K. The second product, based on InAlSb film with a 4.8 micron cut-off, was first introduced this year at the Orlando SPIE conference, operating inside a camera at a temperature of 100 K.

This year SCD is introducing the first detector with a 15-μm pitch and a format of 640×512. SCD's future products will integrate all these technologies together in the same detector, i.e., digital signal processor bonded to antimonide array.

In this paper, we describe the technology and the products in the present and future both for MWIR and for LWIR detection. First, the basic concept and the products of the Sebastian range of detectors will be described. Then, the technology and characterization results of the ABCS program will be presented and future plans will be described.

2. SCD MWIR FPA roadmap

Two dimensional focal plane arrays based on InSb photodiodes bonded to a CMOS readout circuit have been produced in SCD since 1997. The basic InSb technology consists of planar ion implanted photodiodes, hybridized to a Si focal plane processor (FPP) by means of indium bumps, and then backside thinned with surface passivation and anti-reflection coating. The roadmap of the two dimensional FPAs is described in Fig. 1. Three FPAs for the mid format with 30-μm pitch were developed, two of them are based on SCD signal processors (Gemini and Blue Fairy [10]) and one is based on an Indigo signal processor. Since 2000 SCD has been producing larger format FPAs with 640×512 elements and smaller pitch, in which the first two FPAs are based on Indigo ROICs with 25- or 20-μm pitches. Since 2003 SCD has been producing the Sebastian detector which is based on SCD's digital signal processor which has a 20-μm pitch. This detector will be described in more detail in the following section. In order to improve the resolution of the mid format detectors (320×256, 30-μm pitch) SCD has been developing two types of detector which have exactly the same active area as the mid format. The first one belongs to the Sebastian family and has been produced since 2004. It has a format of 480×384 elements

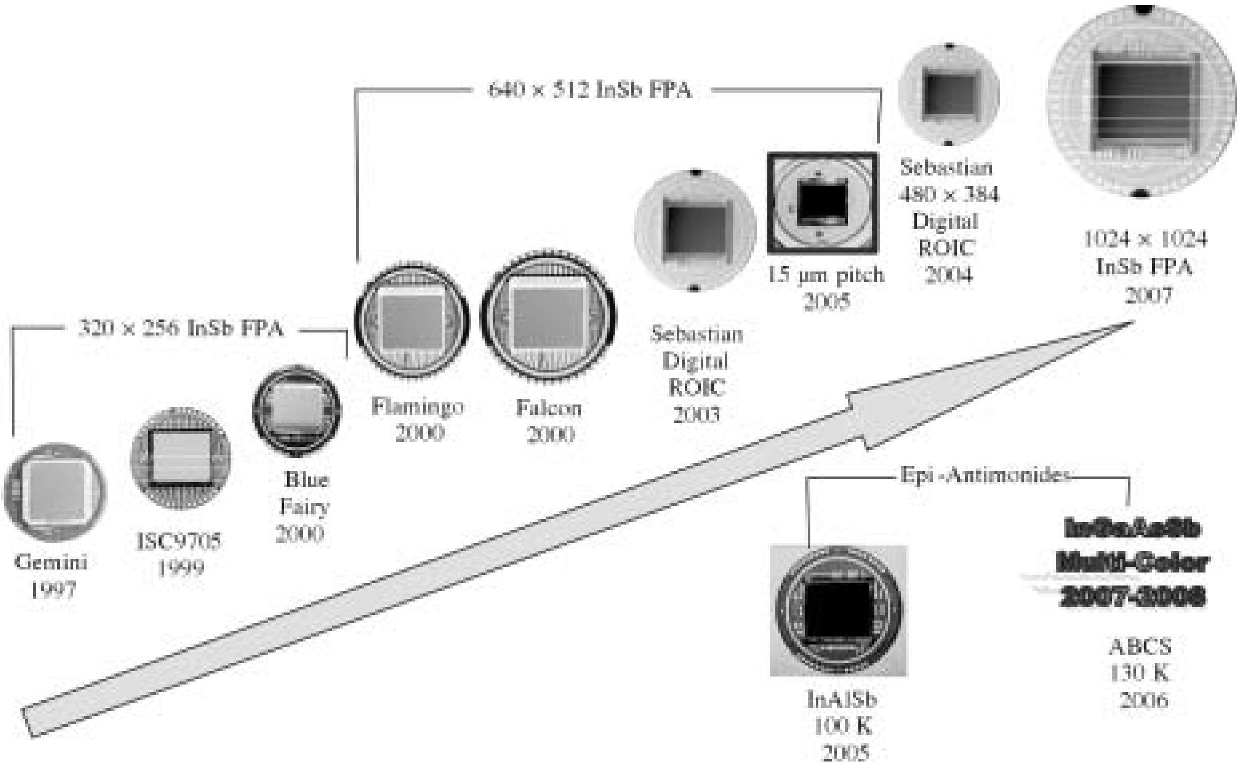

Fig. 1. SCD MWIR 2-D FPA roadmap.

with a 20-μm pitch. The second one has a format of 640×512 elements with a 15-μm pitch. Prototypes of these detectors which are based on the Indigo signal processor ISC0402 will be available this year, and a detector which is based on SCD's digital signal processor will be available next year. Based on the 15-μm technology, SCD will in the future develop detectors with larger formats, such as 1000×1000. In parallel to all these activities, SCD is developing the new technology of the ABCS program which will be described in detail below This year we introduced the first prototypes of InAlSb (with 4.8-μm cut-off) bonded to a Blue Fairy signal processor operating at a temperature of 100 K and integrated inside a hand held camera. By the end of the year, prototypes of InAlSb bonded to Sebastian 480 will be available. In the near future (2006), a detector with an operation temperature above 130 K will be developed, and this detector will have a cut-off of 4.2 μm. On the basis of these technologies a bi/multi-colour detector can be designed for the 3–5 μm regime. For the long term, based on the technology of MBE epitaxial thin films and ABCS, InAs/InGaSb superlattice structures can be designed for any wavelength of operation starting from 3 μm, including 2 dimensional arrays for the MWIR and LWIR regimes.

3. SCD LWIR FPA roadmap

During the 90's, SCD started the development of backside illuminated detectors which are based on $Hg_{1-x}Cd_xTe$ (MCT) for detection in the 8–12 μm regime. These MCT detectors are flip-chip bonded to a signal processor located on the FPA. The technology is based on liquid phase epitaxial (LPE) growth of a MCT layer on a CdZnTe (CZT) substrate and implantation of photodiodes into the epitaxial MCT layer. The first product of this program is a linear array of 256×1 elements which consists of two rows of photovoltaic elements for redundancy. The first prototype of this detector was supplied in 1996 and during the current decade this detector has been produced in high volume with about 5,000 detectors in the field. On the basis of the photovoltaic MCT technology a time delay integration (TDI) detector was developed at SCD, this detector consisting of 480×6 elements which enables the operation of 480×4 at the system level (the four good diodes are chosen out of six) with improved signal to noise for each channel. The 480×6 element TDI detector was integrated successfully into a scanning system demonstrating a high level of performance with high image resolution on the system level. During 2004 SCD finished the development of a smaller format TDI detector with 288×4 elements.

During 2002, SCD started to develop a micro-bolometer detector which is based on VO_x technology. Recently, SCD has demonstrated its first prototype of an uncooled detector which is based on VO_x technology. It is based on a format of 384×288 elements, with a pitch of 25 μm and it exhibits a typical NETD of 50 mK at F/1 [11]. In addition to its high level of radiometric performance, this detector has two unique features, power-save mode for low power consumption and on-line signal drift compensation due to ambient temperature changes, which reduces the need for frequent one point corrections.

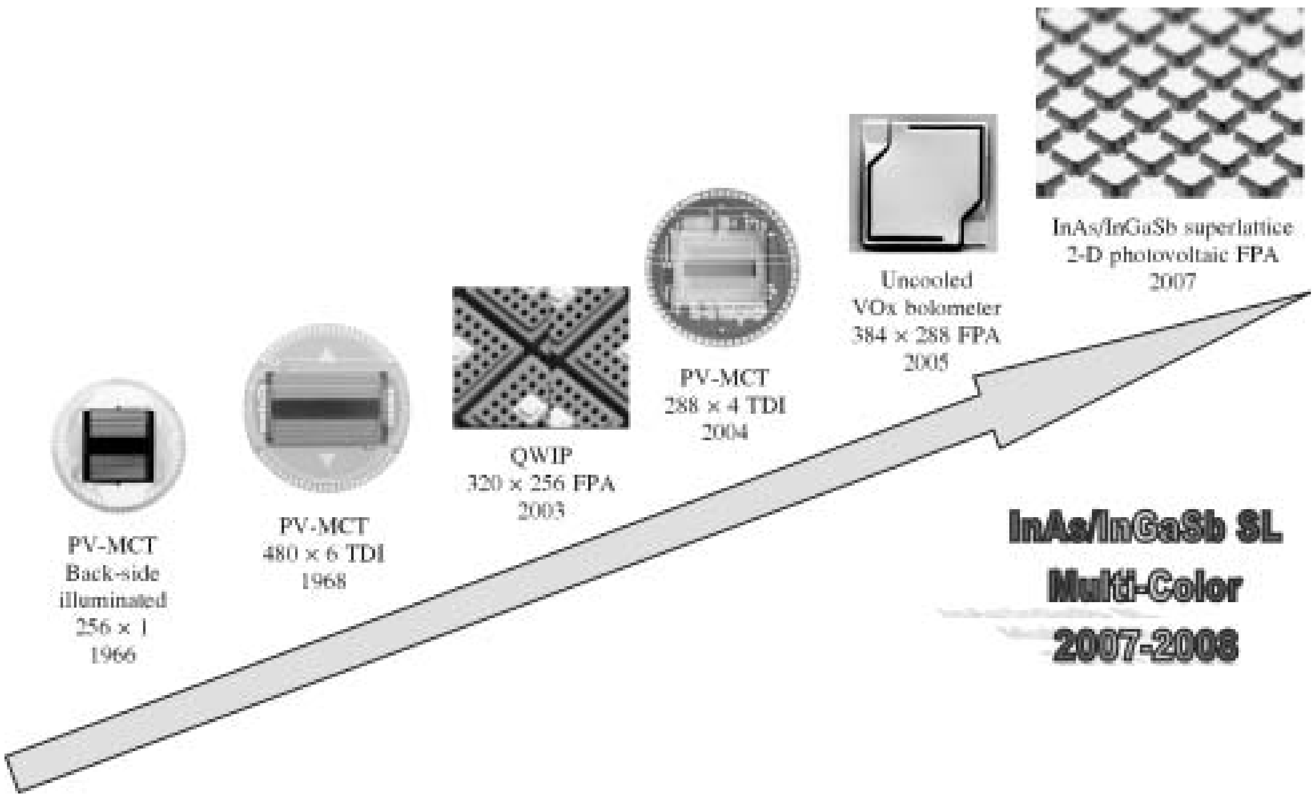

Fig. 2. SCD LWIR FPA roadmap.

Since 2003 SCD has been producing detectors which are based on quantum well infrared photo-detector (QWIP) structures for LWIR detection, according to customer demands. SCD buys the QWIP chip from suppliers, bonds it to a signal processor and integrates in into a Dewar. Based on the ABCS program, SCD is planning to implement future LWIR two dimension arrays with a superlattice made of periodic InAs/InGaSb layers. This device enables the design of detectors which are sensitive to wavelengths from 3 μm up to > 14 μm.

4. SCD digital detectors

During 2003 SCD completed the development of the first detector which is based on a digital signal processor on the focal plane array (FPA) itself. The main challenge in designing a high performance signal processor for a cooled IR detector with digital output was to maintain power consumption similar to that in an analogue processor. Predictions showed that the conventional design for analogue to digital conversion (ADC) results in power consumption over 1 W under the operation conditions of a standard IR detector. However, the special design at SCD of the ADC and the whole signal processor has resulted in a power consumption of the digital signal processor which is even lower compared to existing analogue processors.

Detectors based on a digital FPA are considered to be very attractive due to their many advantages over detectors with an analogue FPA, which are expressed especially on the system level. These include:

- lower level of readout noise due to immunity of the analogue signal to external noise,
- higher linearity,
- less sensitivity to external ambient conditions,
- higher long term stability of the residual non uniformity (RNU),
- removal of the requirement to develop low noise electronics in the system,
- distance between the detector and the system electronics can be increased up to several meters without performance degradations,
- integration of the detector into the system is much simpler and faster.

Over the past two years we have presented at the springtime SPIE conferences two types of our digital detector (Sebastian). The first one with a format of 640×512 in 2003 and the second one with the format of 480×384 in 2004. All the above advantages of digital detectors were demonstrated by the performance measured on the Sebastian detectors.

In this section we present the general structure of the signal processor and its main features, together with some typical performance results that were measured.

4.1. D^{3}C basic structure

The digital focal plane processor (DFPP) is fabricated with a 0.5 μm double-poly, triple metal CMOS process and it consists of 4.5 million transistors. The basic appearance of the digital detector Dewar cooler (D^{3}C) with its proximity card is shown in Fig. 3. A special proximity electronics board was developed for this detector, which consists of a FPGA with a local oscillator. The basic arrangement is shown in Fig. 3, where the FPGA operates the DFPP directly, collects the data from the DFPP, formats it and sends it out to the system. All other system operation modes are controlled by the system via the communication channel including timing of operation. The interface between the FPGA and the system can either be standard (e.g. camera link), or specific as per system requirements. This concept of a simple interface between the D^{3}C and the system leads to easy and fast integration of the D^{3}C into the system.

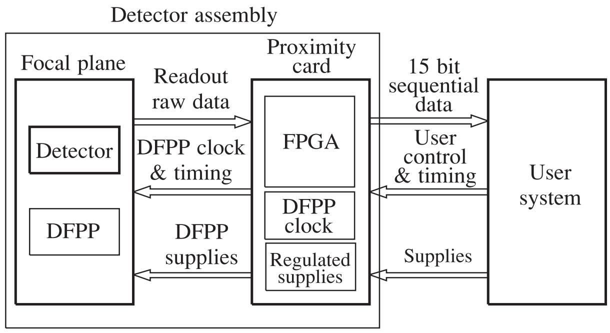

Fig. 3. Block diagram of system-proxy-detector.

4.2. D^{3}C performance

The special design of the signal processor yields an excellent linearity of less than 0.01% deviation/full range over a regime that starts at 2% and continues to 90% well-fill capacity. A direct outcome of this high linearity is a low RNU which is less than 0.015% std/DR for a range of 2–90% well fill capacity. Figure 4 shows the linear relationship between the squared measured noise and the signal which testifies to the clean sampling of the signal inside the FPA due to the onboard A/D conversion in the FPA.

The low level of the total noise achieved with SCD's digital detector enables the attainment of a very good system NETD of 10 mK for 50% well fill capacity. Comparing the spatial and the temporal noise a similar value of 10 mK is achieved in SCD's Digital detectors. The diversity of modes together with the direct control of the FPGA on the detector enables various operational modes which are not available for analogue detectors. For example, the detector can be operated with different integration times for each frame (elaboration of combined mode) where the length and timing of the integration can be changed from frame to frame regardless of the previous frame. The detector can also be operated with multiple integration pulses in the same frame with a pixel saturation level control, this mode enables high dynamic range together with high frame rate detector operation. A TDI mode of operation is also available in the detector with control of the TDI depth to allow operation at different speeds.

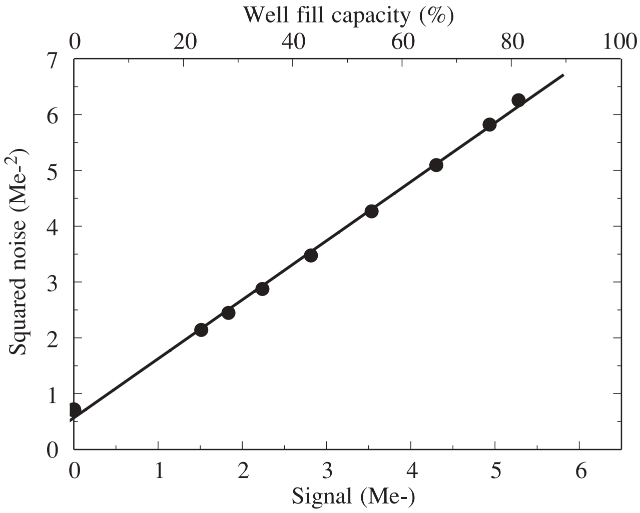

Fig. 4. Squared noise versus signal measurement.

4.3. Main features

In Sebastian, the conversion resolution is controlled externally and can be changed continuously from 12–15 bits. There is a trade off between the conversion resolution and the maximum frame rate, such that a higher frame rate can be achieved with lower resolution. An anti-blooming circuit was implemented at the input stage of the signal processor to avoid a very strong light source from disrupting its operation. All the detectors contain a correlated double sampling (CDS) mechanism inside the signal processor, where the CDS data is read outside and is subtracted from the video data. The use of CDS during operation was found to be very useful for low frequency noise reduction and for NUC stability enlargement. The pixel binning mode is a connection of every two or four adjacent pixels together, which is done inside the signal processor. This feature enables operation with an effective pixel size of 20×40, 40×20 or 40×40 μm. This mode is very useful while trying to detect a sub pixel target where the image is smeared over four pixels (due to the diffraction limitation of the optics) and the signal is very weak. By applying the four pixels merging function the signal to noise improves significantly, compared to the case where an external addition of the data is done at the digital level of the image processing. In the following table there is a comparison between the main features of the two Sebastian detectors and Blue Fairy.

All these features combined with a high level of performance at the system level, make the Blue Fairy and Sebastian detectors the ideal solution for missile warning systems (MWS) [12].

5. Antimonide based detectors

5.1. Introduction

Going beyond the systems described above, SCD's 3rd generation programme is based on epitaxial diode materials. These materials have the potential for higher operating temperatures and multi-band detection. They belong to the antimonide based compound semiconductor (ABCS) family of III-V materials and are based on InAlSb and InAsSb alloys and InAs/InGaSb superlattices. To cover the MWIR atmospheric window, we recently proposed [7] the epitaxial alloys: $InAs_{1-y}Sb_y$ on GaSb with $0.07 < y < 0.11$ and $In_{1-z}Al_z$ Sb on InSb with $0 < z < 0.03$. These can be used together with superlattices based on thin layers of InAs and InGaSb that provide the basis for detector materials operating also in the 8–12 μm long wavelength infra-red (LWIR) atmospheric window as well as in the MWIR [13]. For the alloys, there can be a small lattice mismatch between the alloy and the substrate material, and this can lead to the generation of dislocations inside the alloy. It is therefore necessary to find a strategy to suppress the effect of the dislocations so that they are not harmful to detector operation. On the other hand superlattices, in principle, offer

Table 1. The main features of the Blue Fairy and Sebastian detectors.

Feature	Blue Fairy	Sebastian 480	Sebastian 640
Format	320×256	480×384	640×512
Full range (gain) Me^-	3.5/7/11/15/22/30	1/3/7/10/14	3/7/10/14
Frame rate@full frame	> 450 Hz	>160Hz@15bit >240Hz@13bit >280Hz@12bit	>120Hz@15bit >160Hz@13bit >180Hz@12bit
Main integration modes	ITR/IWR/combined	ITR/IWR/combined/multistep/multiple	
Readout dilution	——	every 2nd and 6th row	every 2nd row
Pixel binning	——	1×2, 2×1, 2×2	
Linearity	<0.05%@2–90% WF	<0.01%@2–90%WF	
RNU std/dr	<0.025%@2–90%WF	<0.015%@2–90%WF	
InSb bias operating point	500 pA – 1 μA	70 pA – 100 nA	70 pA – 100 nA
Windowing	every 2 rows/16 columns	every 2 rows	every 4 rows

the advantage of full wavelength tunability without the disadvantages of limited device thickness or excessive numbers of dislocations.

In the initial stages we have focused in particular on $In_{1-z}Al_zSb$ alloys grown on InSb. Using this approach we have reached in a relatively short time a number of significant breakthroughs. These include 320×256 element mesa FPAs from epitaxial InSb with dark currents at 95 K comparable to those of implanted FPAs at 77 K and mesa FPAs from InAlSb with dark currents up to an order of magnitude lower. For epitaxial InSb the operability and residual non-uniformity (RNU) at 95 K are respectively more than 99.5% and less than 0.03% (standard deviation/dynamic range) after a two point non uniformity correction (NUC). The RNU remains very low even when the operating temperature is allowed to shift quite significantly. This so-called "*V*-curve" stability is a critical performance parameter for harsh environments. For epitaxial $In_{1-x}Al_xSb$ the "*V*-curve" stability increases substantially relative to that in epitaxial InSb due to its lower dark current. In these materials at 90 K we have achieved operabilities greater than 99% in alloys with $x = 0.01$ and 98.8% for $x = 0.03$. Due to the rapid evolution of performance during the development phase we expect that further improvements in the operability of the alloys will soon be achieved.

In the remaining part of this paper we will present some of the key technological achievements for $In_{1-x}Al_xSb$ based FPAs, including both binary and ternary epitaxial materials. Work on InAsSb alloys and InAs/InGaSb superlattices, will be reported in a future publication but some further details may already be found in Ref. 7.

5.2. New FPA materials: epitaxial InSb and InAlSb

InSb and InAlSb layers that are suitable for fabrication into mesa diodes are grown at SCD by molecular beam epitaxy (MBE) on (100) InSb substrates, using a Veeco GEN III MBE machine. The n-type active photon absorbing region

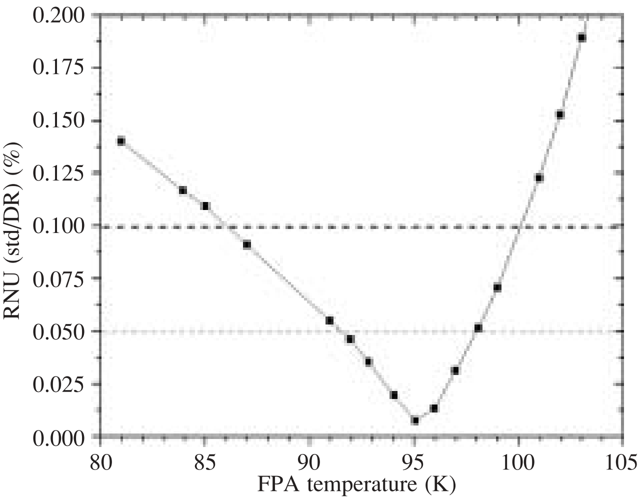

Fig. 5. "*V*-curve" showing RNU of FPA vs. FPA temperature for 2-point NUC performed at 95 K.

is typically 3–5 μm thick and not intentionally doped. The p-side of the junction is typically 1–2 μm thick and is Be doped at $\sim 10^{18}$ cm^{-3}. The epitaxially grown junction and mesa geometry provide some significant advantages over SCD's current planar implanted diode technology including a higher quality of p-n junction with lower dark current, and suppression of blooming and cross talk. In order to exploit this epitaxial material we have developed a new mesa technology. The mesas are highly uniform and are prepared by either dry or wet chemical etching to depths of 2–6 μm.

In the next two sub-sections we present some key performance parameters of our diodes and FPAs, first for epitaxial InSb and then for epitaxial InAlSb with cut off wavelengths up to 1 μm shorter than in the case of InSb.

5.2.1. InSb

FPAs with 320×256 pixels have been fabricated by combining SCD's epitaxial InSb with SCD's Blue Fairy signal processor. The operability of the FPA is greater than 99.5%, both at 80 K and 90 K, based on stringent criteria routinely applied to our production line FPAs which involve the removal of both hard defects and of soft non-uniformity defects. At both of these operating temperatures the FPA has a RNU of < 0.03% for scene temperatures between < 20 C and 75 C after a standard two point correction has been performed. Excellent quality images have been obtained which have been presented previously [14]. The quality remains high even when taken under the following operationally demanding conditions: a two point correction is performed once, at an FPA temperature of 80 K and it is then used to correct the raw signal at 90 K. For scene temperatures from < 20 C to 75 C (< 20% to 90% well fill) the RNU remains below 0.1%, even though the temperatures of calibration and operation differ by ~10 degrees. The dependence of the RNU on FPA temperature is demonstrated explicitly in Fig. 5, which shows a "*V*-curve" of the temperature dependence of the maximum RNU (usually close to 50% well fill) with an integration time of 1.6 mS at F/number 2.5, after a 2-point NUC (~30 and ~60% well fill) is performed at an FPA temperature of 95 K. It shows how the RNU remains below 0.1% for deviations from the 95 K calibration temperature of up to about –10 K and +5 K. The curve demonstrates clearly the very high stability of the FPA performance, even in environments where the FPA temperature may fluctuate strongly. This gives a serious advantage, for example in missile applications, where the good RNU stability is a critical issue.

Figure 6 shows the distribution of the dark currents in the FPA pixels at 90 K. It may be seen that the distribution is very narrow with a peak value of 4.2 pA and a full width at half maximum (FWHM) of 0.4 pA. The high stability of the RNU at 95 K against temperature variations of ~10 K is a direct consequence of the high uniformity of the diodes and the narrowness of their dark current distribution 15.

The FPA operating temperature can be increased above 90 K before the dark current grows to a level where it be-

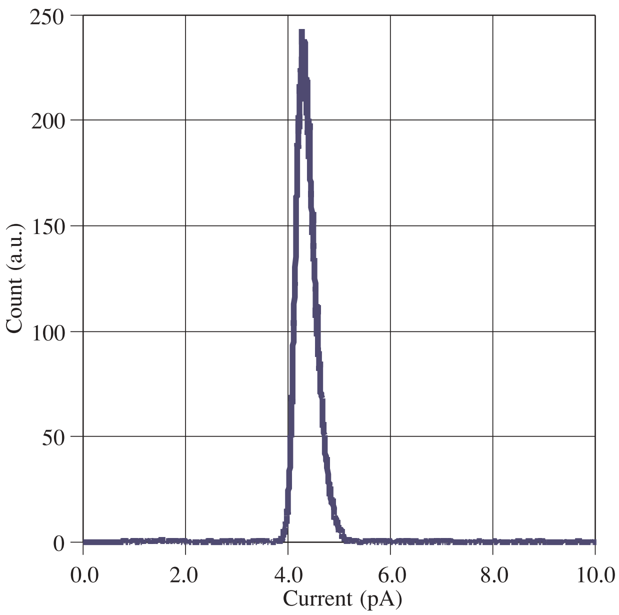

Fig. 6. Distribution of dark currents at 90 K and at a bias of –168 mV in the pixels of an InSb FPA (peak = 4.2 pA, FWHM = 0.4 pA, operability 99.6%).

gins to degrade the performance seriously. For example an image taken at 110 K is shown in Fig. 7. Even at this temperature, the definition remains high and power lines at a range of 2 km are still visible. Such performance at high operating temperature provides benefits for example in hand-held and sighting applications, since it allows significant power savings to be made, an issue which can sometimes be critical.

5.2.2. InAlSb

The bandgap of $In_{1-x}Al_xSb$ is expected to increase at roughly 18 meV for every 1% of Al, based on a simple linear interpolation between the bandgap of InSb and the direct bandgap of AlSb. This increase provides additional

Fig. 7. Image recorded with the 256×320 pixel InSb mesa-FPA at a focal plane temperature of 110 K.

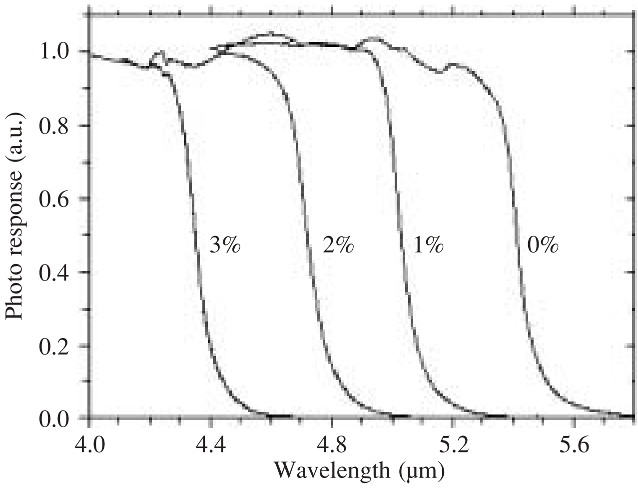

Fig. 8. Photoresponse spectra for InAlSb diodes at 77 K with λ_C from 5.4 µm (InSb) to 4.4 µm.

suppression of the dark current over that possible in high quality epitaxial InSb diodes.

In Fig. 8, we show the photo-response of several InAlSb diodes where the aluminium composition increases from right to left. The decrease in the cut-off wavelength with increasing Al composition may be seen clearly, from λ_C ~5.4 µm for InSb to a value of λ_C ~4.4 µm for the 3% alloy. The steepness of the absorption edge is similar in all cases without any significant signs of degradation. Figure 8 shows the ease with which the bandgap and cut-off wavelength of our FPAs can be tuned by varying the aluminium composition.

In the following two subsections we demonstrate the effect of alloying on diode performance. Below we present results of dark current measurements on single diodes and the collective diode performance for whole FPAs.

Single diode properties

Figure 9 shows the dark current at a reverse bias of –100 mV as a function of temperature between 77 K and 180 K for a representative 50×50 µm InAlSb diode with λ_C ~5.0 µm. In the figure, the logarithm of the current is plotted as a function of the inverse temperature. The slope for a purely GR limited diode should be approximately equal to $E_G/2k$, where E_G is the low temperature value of the energy bandgap of the semiconductor, while for diffusion it should be nearly equal to E_G/k. The two straight lines indicated in the figure correspond to activation energies of E_G ~ 270 meV for the upper line and $E_G/2$ ~140 meV for the lower line. These values correspond quite well with the expected bandgap and show clearly that the lower temperature region with the lower slope is dominated by GR while the higher temperature region with the steeper slope is dominated by diffusion. The changeover from GR to diffusion occurs at a temperature of about 130 K.

The low dark current for single diodes at 90 K that may be derived from Fig. 9 is a necessary condition for good FPA performance. However, as already mentioned above,

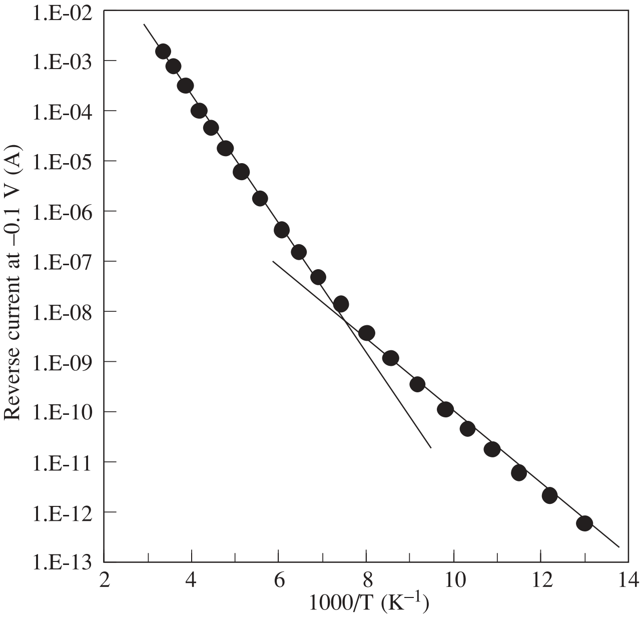

Fig. 9. Arrhenius plot of reverse current at a bias of –100 mV for an InAlSb diode with λ_C ~ 5.0 µm. The straight lines have activation energies of ~140 meV and ~270 meV, respectively.

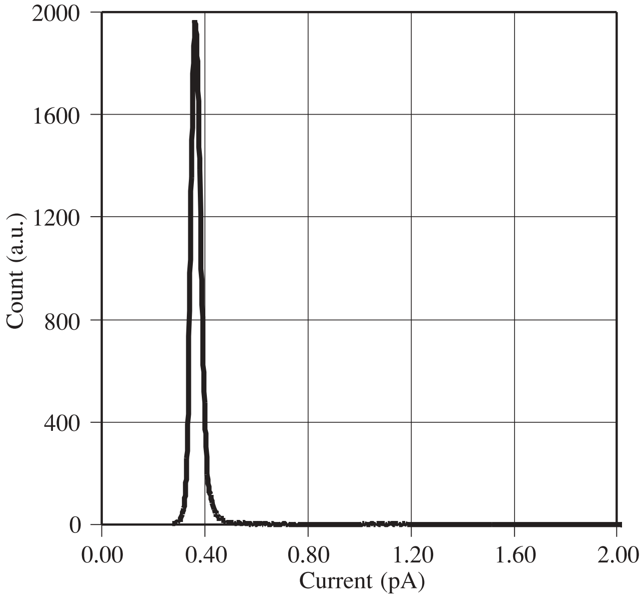

Fig. 10. Distribution of dark currents at 90 K and at a bias of –309 mV in the pixels of an InAlSb FPA, λ_C ~4.4 µm (peak = 0.36 pA, FWHM = 0.03 pA, operability 99.1%).

it is also critical that the distribution of dark currents of all of the FPA diodes is as narrow as possible, in order to get a very low and stable value for the detector RNU, both at 90 K and above. This in turn requires a high uniformity in the aluminium composition. We shall demonstrate that a very uniform composition and a very narrow distribution of dark currents can be achieved.

FPA properties

Many 320×256 InAlSb FPAs have been made using SCD's Blue Fairy silicon processor. For a cut-off of λ_C ~5 µm typical dark currents at 90 K are 1.5–2.5 pA. Operabilities of 99% or better at 90 K can be achieved, based on the same selection criteria as described above for InSb. In these cases, the full width at half maximum (FWHM) of the dark current is typically about 200–300 fA. This is less than the FWHM reported above for epitaxial InSb and is well within the range required to provide excellent temperature stability of the FPA, as already discussed in Sect. 5.2.1. When the cut-off wavelength is further reduced to λ_C ~4.4 µm, the dark current is lowered to ~250 fA and the FWHM to ~30 fA. This is demonstrated in Fig. 10. In fact, the most striking feature of the dark current distributions in our InAlSb FPAs is that their relative widths are essentially constant for the full range of cut-off wavelength up to λ_C ~4.4 µm ($0 < x < 0.03$), that is 1–13% of their peak dark current values.

From a technological point of view, the satisfying outcome of the tight dark current distributions described above is that by going to a more complex ternary material it is possible to gain the benefits of bandgap tunability with almost no penalty in uniformity, both at the material and process level. Applying the method described in Ref. 14 to analyse the dark current distribution, we can show that for $x = 0.03$, the $In_{1-x}Al_xSb$ alloy composition across the FPA has a standard deviation that must lie below 0.0005.

The dependence of the mean FPA dark current at a bias of approximately –150mV and FPA temperature of 90 K is shown in Fig. 11 as a function of cut-off wavelength (composition range: $0 < x < 0.03$). The results are compared with the theoretical expectation for a constant number of GR centres, N_{GR}: $I_d = aN_{GR}\exp(-hc/2\lambda_C kT)$ where a is a constant of proportionality, and the agreement is found to be quite good. This shows that increasing the aluminium composition does not significantly increase the number of GR centres. The dark current thus decreases essentially as expected from a simple increase in the bandgap. The technological implications of this behaviour are significant, since it provides the basis for two colour detectors made with stacked diodes, each with a different composition.

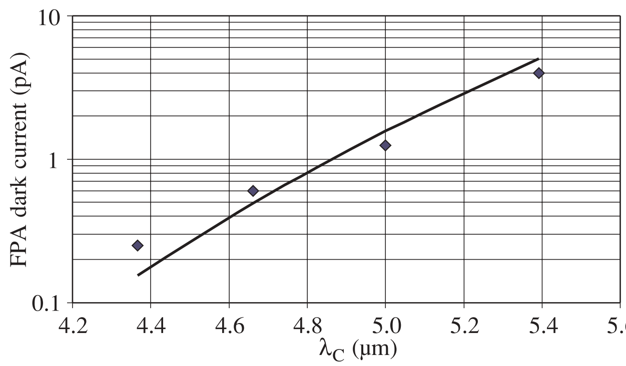

Fig. 11. Dependence of mean dark current at a bias of about –150 mV and at an FPA temperature of 90 K on cut-off wavelength ($0 < x < 0.03$). Points are mean dark current values. Line is fit to GR formula for a constant number of GR centres.

After a two-point NUC, the RNU of an InAlSb FPA with λ_C ~5 μm is typically less than 0.01% between 26% and 75% well fill. In Fig. 12, we compare the *V*-curve for the InSb FPA of Fig. 5 with a *V*-curve for such an InAlSb FPA. The conditions are slightly different in that the integration time has been increased to 4 mS without changing the well-fill. This naturally narrows the width of the *V*-curve (due to the lower photocurrent conditions) but is sufficient for a straight comparison between the two FPA compositions. It can be seen that the *V*-curve for the InAlSb FPA has nearly doubled the width of that for the InSb FPA. This can be explained in terms of the lower absolute width of the dark current distribution in the alloy FPA. In Fig. 13, we present an image measured with an InAlSb FPA with λ_C ~5 μm operated at 100 K, in order to demonstrate the high quality of the image that can be produced.

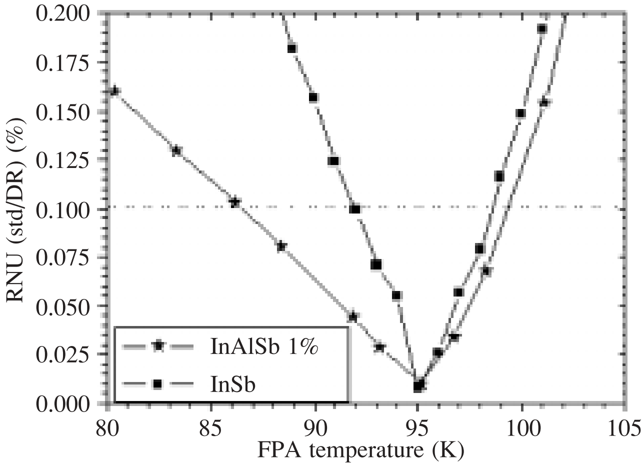

Fig. 12. *V*-curves for the FPA of Fig. 5 and an FPA made from $In_{0.99}Al_{0.01}Sb$. The integration time is 2.5 times longer than in Fig. 5, resulting in a narrower opening of the "*V*".

6. Conclusions

Today semi-conductor devices (SCD) has a high production capability of over 5800 IR detectors per year. Presently, SCD products are based on both InSb technology for MWIR two dimensional array detectors and mercury cadmium telluride technology for LWIR time delay and integration detectors. All these technologies are provided by a full suite of in-house facilities such as: crystal growth, full chip processing including flip-chip bonding, VLSI design, FPA integration within the Dewar with either Stirling or JT cooling, and full detector characterization. This complete capability at each stage of production allows total optimization of the integrated detector to achieve the best performance. Large numbers of SCD IR detectors are used in a variety of applications such as high quality imagers, hand held cameras, seeker heads, targeting pods, and air reconnaissance. SCD's revolutionary high performance digital detector, the only one of its kind, is spearheading a new family of detectors (640×512, 480×384, and 320×256) which can be integrated very quickly into the system, and which provide excellent performance at the system level including: low noise, low residual non uniformity (RNU) with long term stability, and high linearity of response. In this paper, we have presented details of our new ABCS mesa FPAs, based on epitaxial InSb and InAlSb layers grown in-house by MBE. We have been able to demonstrate a very high degree of alloy uniformity, with a standard deviation in composition of $\sigma_z \leq 0.0005$ for $In_{1-z}Al_zSb$ with a wavelength cut-off close to 5 μm. We have demonstrated a radiometric performance and stability in InSb FPAs at 95 K comparable to that previously only achievable at 77 K, and we have presented high quality images for FPAs made from both binary and alloy materials operating up to 110 K. We are confident that by connecting the FPAs developed within SCD's ABCS program to SCD's recently developed Digital FPP, we shall be able to provide our customers with maximum performance advantage, both at the level of the diode material and at the level of the processor.

Fig. 13. Image produced by InAlSb FPA at focal plane temperature of 100 K.

Acknowledgements

The authors, first and foremost, would like to acknowledge the many technicians, engineers and scientists of SCD without whose long and dedicated work the products and research described in this review would never have been realized. We gratefully acknowledge the close and continuing collaboration with the Soreq NRC and also their assistance with the photoluminescence measurements presented in this article. We also thank the Israeli MOD for their support.

References

1. O. Nesher, P.C. Klipstein, and E. Weiss, "Advanced IR detector design at SCD: from D^3C^{TM} to ABCS", *Proc. SPIE* **5359**, 101–110 (2004).
2. T. Markovitz, F. Schapiro, D. Alfiya, S. Hasson, A. Magner and O. Nesher, "Piccolo – a high performance IR detector

optimized for handheld applications", *Proc. SPIE* **5406**, 239–248 (2004).
3. M. Zucker, I. Pivnik, E. Malkinson, J. Haski, T. Reiner, D. Admon, M. Keinan, M. Yassen, I. Sapiro, L. Bykov, N. Sapir, and A. Fraenkel, "Long, mid-wave infrared detector with time delayed integration", *Proc. SPIE* **4820**, 580–592 (2002).
4. S. Elkind, A. Adin, I. Nevo, and A.B. Marhasev, "Focal plane processor with a digital video output for InSb detectors", *Proc. SPIE* **4820**, 751–757 (2002).
5. O. Nesher, S. Elkind, A. Adin, I. Nevo, A.B. Yaakov, S. Raichshtain, A.B. Marhasev, A. Magner, M. Katz, T. Markovitz, D. Chen, M. Kenan A. Ganany, J.O. Schlesinger, and Z. Calahorra, "A digital cooled InSb detector for IR detection", *Proc. SPIE* **5074**, 120–129 (2003).
6. O. Nesher, S. Elkind, I. Nevo, T. Markovitz, A. Ganany, A.B. Marhashev, and M. Ben-Ezra, "480×384 element InSb detector with digital processor", *Proc. SPIE* **5406**, 214–221 (2004).
7. P. Klipstein, E. Jacobson, O. Klin, M. Yassen, Z. Calahora, E. Weiss, S. Risemberg, and D. Rosenfeld, "Antimonide based materials for infrared detection" *Proc. SPIE* **4820**, 653–662 (2002).
8. P. Klipstien, Z. Calahora, A. Zemel, R. Gat, E. Harush, E. Jacobson, O. Klin, M. Yassen, J. Oiknine-Schlesinger, E. Weiss, and S. Risemberg, "Third-generation infrared detector program at SCD", *Proc. SPIE* **5406**, 222–229 (2004).
9. P. Klipstien, Z. Calahora, A. Zemel, R. Gat, E. Harush, E. Jacobson, O. Klin, M. Yassen, J. Oiknine-Schlesinger, E. Weiss, and S. Risemberg, "3rd generation infrared detectors at SCD: InAlSb focal plane arrays", *Proc. SPIE* **5406**, 222–229 (2004).
10. O. Nesher, S. Elkind, A. Adin, U. Palty, O. Pelleg, E. Jacobsohn, T. Markovitz, I. Szafranek, Z. Calahorra, and J. Oiknine-Schlesinger, "Performance of BF focal plane array 320×256 InSb detectors", *Proc. SPIE* **4820**, 699–707 (2002).
11. U. Mizrahi, A. Fraenkel, L. Bykov, A. Giladi, A. Adin, E. Ilan, N. Shiloah, E. Malkinson, Y. Zabar, D. Seter, R. Nakash, and Z. Kopolovich, "Uncooled detector development program at SCD", *Proc. SPIE* **5783**, 551–558 (2005).
12. O. Nesher, S. Elkind, and T. Markovitz, "Advantages of SCD detectors for missile warning system", *Proc. SPIE* **5612**, 32–41 (2004).
13. A. Fuchs, L. Bürkle, R. Hamid, N. Herres, W. Pletschen, R.E. Sah, R. Kiefer, and J. Schmitz, "Optoelectronic properties of photodiodes for the mid- and far-infrared based on the InAs/GaSb/AlSb materials family", *Proc. SPIE* **4288**, 171–182 (2001).
14. P. Klipstien, Z. Calahora, A. Zemel, R. Gat, E. Harush, E. Jacobson, O. Klin, M. Yassen, J. Oiknine-Schlesinger, and E. Weiss, "Third-generation infrared detector program at SCD: InAlSb focal plane arrays", *Proc. SPIE* **5612**, 42–50 (2004).
15. L. Shkedy, O. Amir, Z. Calahorra, J. Oiknine-Schlesinger, and I. Szafranek, "Temperature dependence of spatial noise in InSb focal plane arrays", *Proc. SPIE* **4028**, 481–488 (2000).

